J. Fluid Mech. (1969), *vol.* 38, *part* 4, *pp.* 769–791
Printed in Great Britain

The dynamical instabilities of cylindrical shells

By J. P. SOMON
Laboratori Gas Ionizzati del C.N.E.N., Frascati, Italy

(Received 24 October 1968 and in revised form 18 April 1969)

Collapsing cylindrical metallic shells have been used to compress magnetic fluxes and generate megagauss magnetic fields. Such shells experience large, rapidly growing accelerations and their symmetry can be completely destroyed by Rayleigh–Taylor instabilities. This paper presents a theoretical study of the Rayleigh–Taylor instability for radially accelerated incompressible cylindrical shells submitted to the pressure of much lighter media. Low-amplitude flute perturbations are considered and Fourier-analyzed in the azimuthal angle. A fourth-order linear differential system with time-dependent coefficients is derived, which determines the two interface-displacements. Stability criteria are discussed. When the perturbation wavelength is much greater or much smaller than the shell thickness, the differential system splits into two independent differential equations and results are greatly simplified; analytical solutions are available for some cases.

The case of axial field compression (A.F.C.) is discussed as an application. Numerical solutions give the time behaviour of all possible initially given disturbances. The initial perturbations, which are able to reach the axis during their development and which are consequently dangerous in magnetic field compression experiments, have been calculated. Results are consistent with the few experimental data available. They show that the degree of symmetry of cylindrical devices has to be extremely good in order to get successful compressions.

Finally, non-linear and compressibility effects have been taken into account for some A.F.C. cases, solving the full non-linear fluid equations numerically.

1. Introduction

As reported in the proceedings of two conferences on high magnetic field generation and in many other publications,† magnetic fields of the order of several megagauss have been obtained experimentally by means of explosive-driven cylindrical implosions. In such devices, an axial magnetic field is initially generated within a thin hollow metallic cylinder called the 'liner'. A ring of high explosives placed around the liner is detonated on the periphery. Consequently the liner is radially imploded and reaches high velocities during the very

† *Proceedings of a Conference on Megagauss Magnetic Field Generation by Explosives and Related Experiments*, Frascati 1965. (EURATOM 2750e: Brussels, 1966); *Colloque international sur les champs magnétiques intenses, leur production et leurs applications*, Grenoble 1966 (C.N.R.S.: Paris). A detailed bibliography on the subject can be found in Somon (1968*b*).

short expansion time of detonation products. The liner then compresses the magnetic field, which, if no diffusion process occurs (infinite electrical conductivity of the liner), behaves as a polytropic, adiabatic gas with $\gamma = 2$ and negligible mass. The growing magnetic pressure $P_1 = B^2/8\pi \sim r_1^{-4}$ exerted by the field on the inner liner-boundary stops the liner motion at a time t_m (see figures 1, 3). A maximum field B_m is then reached for a minimum or turn-around radius of the inner liner boundary, say $r_1 = r_m$. An outwards decompressive motion follows the compression period. Assuming a perfect cylindrical symmetry of the system, Lehner, Linhart & Somon (1964) and Somon (1965, 1968*b*) calculated the efficiency of this flux compression and derived some limitation to the maximum obtainable field due to the liner compressibility, and to the field diffusion within the liner. It was concluded that it would be extremely difficult to obtain fields greater than 20 MG.

As the implosion symmetry cannot initially be made perfect, it was soon felt, after the preliminary theoretical work of Linhart (1961) and Harris (1962), and after the first experimental results, that a motion-instability might destroy the liner before the maximum field could be reached and therefore provide another essential limitation to the process. The inner liner boundary is an interface between an infinitely light medium (field) and a heavy one (liner). At the vicinity of the maximum compression the interface acceleration is directed towards the heavy medium and the well-known Rayleigh–Taylor instability will then build up on the interface. A proof of the importance of instabilities is given experimentally by the correlation between successful reproducible compressions and the accuracy of the explosive-device symmetry. Unfortunately data on the instability development are still very poor, since optical observation of the inner interface is available only as long as the liner inner radius is relatively large; it shows that the implosion symmetry remains quite good during the observation period, which is consistent with the small deceleration (roughly, $\ddot{r}_1 \sim r_1^{-3}$). At the vicinity of the turn-around radius, i.e. when the deceleration and the related instability suddenly become important, information is obtainable only from magnetic probe-signals. Nevertheless interpretation of these signals suggests some instability mechanism. In most cases the magnetic signal is abruptly interrupted before the field reaches a maximum value, even when the probe radius is smaller than the expected liner turn-around radius; this could be attributed to premature probe destruction due to an excessive development of a liner asymmetry. Di Gregorio, Herlach & Knoepfel (1966) also observed magnetic signals with a maximum field, and found some dispersion in the 'turn-around behaviour', which they attributed to instabilities. Until now magnetic fields up to values of about 6 MG have been reproducibly generated; higher fields, associated with higher liner accelerations, have only been produced in an erratic way. Clearly, the Rayleigh–Taylor instability of the liner motion is a main feature for magnetic flux compression experiments. The purpose of this paper is to study theoretically the Rayleigh–Taylor instability development and, especially, to determine the initial perturbations which lead to a complete destruction of the liner symmetry, i.e. to an interruption of the compression process.

The Rayleigh–Taylor instability (Rayleigh 1900, Taylor 1950) of a two-fluid

interface, submitted to a constant gravity or acceleration, has been studied extensively in plane geometry. Much of the early work is summarized by Chandrasekhar (1961) and Wehausen & Laitone (1960). The simplest case of an incompressible, ideal medium has been generalized by several authors, taking into account fluid stratification, viscosity, surface tension and magnetic field. Kruskal & Schwarzschild (1954) considered also a magnetic-plasma medium. Most studies assume low-amplitude perturbations which make it possible to use a linear analysis, but Birkhoff (1956) and Emmons, Chang & Watson (1960) developed some simplified non-linear theory. Harlow & Welch (1966) solved the Navier–Stokes equations of the problem numerically.

In other geometries the unperturbed motion enters in a more complicated way and the studies are fewer. Spherical bubbles in an infinite medium have been considered by Plesset (1954) and a moving cylindrical interface by Jarem & Watson (1962). The stability of an infinitely thin cylindrical shell has also been investigated, using a normal mode analysis applicable to the modes which grow faster than the characteristic motion time (Linhart 1961, Harris 1962).

In the experimental axial field compression case considered, the geometrical effect is important (small turn-around radius), the liner thickness varies widely during the motion (approximate volume conservation) and the normal mode method cannot always be used with a rapidly growing acceleration. None of the preceding studies known covered this case and the analysis presented here proved to be necessary.

With the exception of § 7, the following main hypotheses will be used in the paper. (i) *The liner is an ideal fluid.* In practice, the pressure tensor is isotropic (Al'tschuler 1965) at the megabar pressures created by compressed magnetic fields. Champetier *et al.* (1965) showed that viscosity and superficial tension are negligible for the considered perturbation wavelengths. (ii) *The liner is incompressible.* (iii) *Instabilities are of a flute type.* These are the most dangerous instabilities, since they do not bend the magnetic lines of force (Harris 1962). (iv) *Perturbations are of low amplitude (linear theory).* Effects due to the liner compressibility and to the non-linearity are discussed and taken into account in § 7.

2. The unperturbed motion

In the presence of an axial magnetic field $\mathbf{B} = B(r,t)\,\mathbf{e}_z$, the equations for an incompressible ideal fluid have the purely hydrodynamical form,

$$\boldsymbol{\nabla}.\mathbf{v} = 0, \tag{2.1}$$

$$\frac{\partial \mathbf{v}}{\partial t} + (\mathbf{v}.\boldsymbol{\nabla})\,\mathbf{v} + \frac{1}{\rho}\boldsymbol{\nabla}P = \frac{(\mathbf{B}.\boldsymbol{\nabla})\,\mathbf{B}}{4\pi\rho} = 0, \tag{2.2}$$

where $P = p + B^2/8\pi$ is the total pressure. For the considered radial motion of a cylindrical circular shell (figure 1) they reduce to

$$r\dot{r} = a(t), \tag{2.3}$$

$$\ddot{r} = -\frac{1}{\rho}\frac{\partial P(r,t)}{\partial r}, \tag{2.4}$$

with $$(\dot{}) = \left(\frac{\partial}{\partial t} + v\frac{\partial}{\partial r}\right)(\ ).$$

Integrating between the two boundaries, one gets

$$r_2^2 - r_1^2 = s^2 = c^t, \tag{2.5}$$

$$\dot{a}\log\frac{r_1}{r_2} + \frac{a^2}{2}\left(\frac{1}{r_1^2} - \frac{1}{r_2^2}\right) + \frac{P_1 - P_2}{\rho} = c^t, \tag{2.6}$$

which determine the inner boundary motion, taking $a(t) = r_1\dot{r}_1$. All other quantities are successively obtained. Useful ones, relative to the outer boundary, will be

$$\frac{r_2}{r_1} = \sigma = \left(1 + \frac{s^2}{r_1^2}\right)^{\frac{1}{2}}, \quad \frac{\dot{r}_2}{\dot{r}_1} = \sigma^{-1}, \tag{2.7}$$

$$\frac{\ddot{r}_2}{\ddot{r}_1} = \sigma^{-1}\left[1 + (1 - \sigma^{-2})\frac{\dot{r}_1^2}{r_1\ddot{r}_1}\right].$$

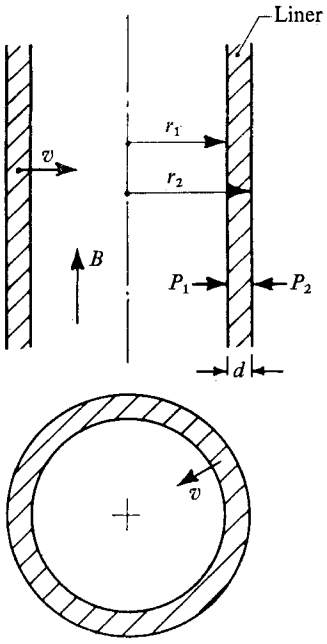

FIGURE 1. The unperturbed cylindrical motion.

Accelerations are essential for Rayleigh–Taylor instability. Considering the time derivative of (2.3) it is easy to find that, inside the liner, the acceleration $\ddot{r}$ has either a constant sign or a single zero for which $\partial\ddot{r}(r,t)/\partial r > 0$. It follows from (2.4) that at any time (i) the pressure P is monotonic, or has at most one

extremal inside the liner (this extremal is always a maximum); (ii) the acceleration vectors $\ddot{\mathbf{r}}_1$ and $\ddot{\mathbf{r}}_2$ on the boundaries cannot be directed simultaneously towards the liner. Hence three possible configurations, which depend on the interface acceleration signs, have been distinguished in figure 2. If an extrapolation of elementary plane stability criteria were allowed, these configurations should be directly related to the motion stability. A liner submitted to the pressures P_1 of lighter media should be stable only for the configuration 2. This will be proved at least for short wavelengths or quickly growing perturbations.

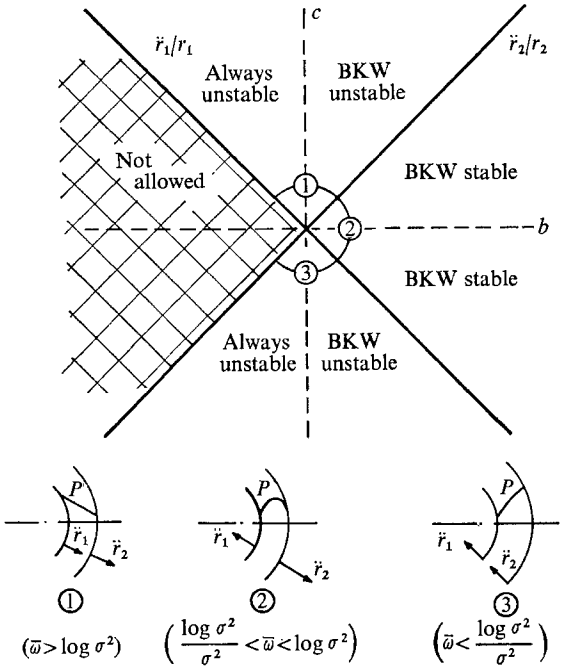

FIGURE 2. The stability in connexion with motion configurations. Configurations depend on the reduced quantities $\bar{\omega} = (P_1 - P_2)/\frac{1}{2}\rho v_1^2 + 1 - \sigma^{-2}$ and $\sigma = r_2/r_1$.

Axial field compressions

The detonation products act as a pressure pulse, which accelerates the liner within a time short compared with the compression time. The liner motion will be considered only after this short acceleration period.† Consequently the explosive pressure $P_2(t)$ will be neglected and the relative boundary condition replaced by a given initial liner velocity $\dot{r}_1(0) < 0$. The axial magnetic field B exerts the pressure

$$P_1 = \frac{B^2}{8\pi} = \frac{B^2(0)}{8\pi}\left[\frac{r_1(0)}{r_1(t)}\right]^4 \tag{2.8}$$

† Some special instabilities or jets created by the pressure pulse are thus ignored but have been studied by Champetier *et al.* (1965).

on the inner boundary, assuming that the liner is a perfect electrical conductor† (constant trapped magnetic flux $\phi = \pi r_1^2 B$).

The A.F.C. motion has been studied by Somon (1965). The use of the reduced quantities

$$\bar{r} = \frac{r}{r_1(0)}, \quad \bar{t} = \frac{|\dot{r}_1(0)|}{r_1(0)} t, \tag{2.9}$$

$$D = \frac{r_2(0) - r_1(0)}{r_1(0)} \approx \frac{\bar{s}^2}{2}, \quad N = \frac{B^2(0)}{8\pi\rho \dot{r}_1^2(0)} \tag{2.10}$$

is convenient. In practice the parameters D and N are such that $N \ll D \ll 1$. The motion equation (2.6) gives the energy conservation law

$$(\bar{r}_1 \dot{\bar{r}}_1)^2 \log\left(1 + \frac{2D}{\bar{r}_1^2}\right) - \log(1+2D) + 2N\left(\frac{1}{\bar{r}_1^2} - 1\right) = 0. \tag{2.11}$$

Thus the magnetic field is compressed until a value B_m, for which a minimum or 'turn-around' radius $r_1 = r_m$, with

$$\bar{r}_m^2 = \frac{B(0)}{B_m} \approx \frac{N}{D} \ll 1, \tag{2.12}$$

is reached. The motion is then reversed, and starts to diverge.

During a long phase of the converging motion, velocities vary very slowly and the boundary accelerations remain consequently small:

$$\ddot{\bar{r}}_1(0) = \bar{r}_m^2 - D, \quad \ddot{\bar{r}}_2(0) = \bar{r}_m^2 + D \ll 1.$$

A very high acceleration peak,

$$\ddot{\bar{r}}_{1m} = \sigma_m \ddot{\bar{r}}_{2m} = (\sigma_m^2 - 1)/\bar{r}_m \log \sigma_m^2 \gg 1,$$

follows which stops the liner within a short time $\bar{t}_c \sim \bar{r}_m$ and will greatly influence the instability development (table 1 and figure 3). For thin enough liners ($D < N^{\frac{1}{2}}$ or $\sigma_m < 3^{\frac{1}{2}}$) the configuration is of type 1 (see figure 2) during the whole motion. For thicker liners the configuration is initially 2 and becomes 1 close to the maximum compression. Initially thin liners will generally be thick at the time $\bar{t}_m$ of maximum compression (typically $\sigma_m = (1 + 2D^2/N)^{\frac{1}{2}} \sim 1{\cdot}5$ to 6). Nevertheless it is interesting to consider the case of an infinitely thin liner for which

$$\bar{r}^3 \ddot{\bar{r}} \approx \bar{r}_m^2, \quad \bar{r}^2 \approx \bar{r}_m^2 + (\bar{t} - 1)^2. \tag{2.13}$$

In this rough approximation maximum accelerations are somewhat underestimated but the trajectory is a simple hyperbola.

3. The perturbed motion

3.1. *The perturbed equations*

In obvious notation the perturbed velocity and pressure are

$$\tilde{\mathbf{v}}(\mathbf{r}, t) = \mathbf{v}(\mathbf{r}, t) + \delta\mathbf{v}, \quad \tilde{P}(\mathbf{r}, t) = P(\mathbf{r}, t) + \delta P.$$

† To allow a diffusion of the magnetic field within the liner should not alter the following instability calculations, which are expressed in terms of the total pressure P, but only complicate the determination of the unperturbed motion $r_1(t)$ (see Somon 1965).

	Case				
	A	*B*	*C*	*D*	*E*
D	0·04	0·1	0·01	0·04	0·04
$(N/D)^{\frac{1}{2}} = \bar{r}_m$	0·1	0·1	0·1	0·25	0·05
$t = 0$					
$\ddot{\bar{r}}_1/\bar{r}_1$	−2·81 (−2)	−7·94 (−2)	2·73 (−4)	2·84 (−2)	−3·57 (−2)
$\ddot{\bar{r}}_2/\bar{r}_2$	4·38 (−2)	7·78 (−2)	1·96 (−2)	9·60 (−2)	3·67 (−2)
$t = t_m$					
$\bar{t}_m$	0·88	0·82	0·94	0·88	0·86
σ_m	3·02	4·65	1·73	1·51	5·63
$\ddot{\bar{r}}_1/\bar{r}_1$	3·56 (2)	5·91 (2)	1·81 (2)	2·56 (1)	2·87 (3)
$\ddot{\bar{r}}_2/\bar{r}_2$	3·90 (1)	2·77 (1)	6·04 (1)	1·11 (1)	9·68 (1)
$g_m = \xi_1(\bar{t}_m)/r_m (p = 2)$					
(1, 0, 0, 0)	−2·6 (2)	−1·2 (2)	−7·0 (2)	−2·6 (1)	−5·7 (2)
(0, 1, 0, 0)	3·6 (2)	1·9 (2)	8·9 (2)	6·7 (1)	7·2 (2)
(0, 0, 1, 0)	2·7 (2)	1·3 (2)	7·1 (2)	3·2 (1)	5·8·(2)
(0, 0, 0, 1)	−3·5 (2)	−1·8 (2)	−8·7 (2)	−6·2 (1)	−7·1 (2)

TABLE 1. The values of some parameters relative to unperturbed motions and to the stability of four harmonic 2 modes. (n) means $\times 10^n$

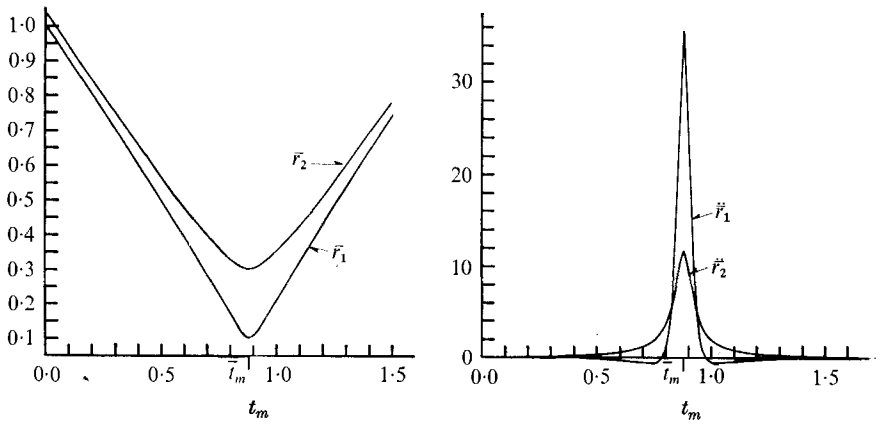

FIGURE 3. Motion law and accelerations for A.F.C.
Case A: $\bar{r}_m = 0{\cdot}1$, $D = 4 \times 10^{-2}$.

A perturbed velocity potential $\delta\phi(\mathbf{r}, t)$ is defined, assuming curl-free initial perturbations. It follows that $\delta\mathbf{v} = \nabla\delta\phi$ with

$$\nabla^2\delta\phi = 0, \tag{3.1}$$

from incompressibility equation (2.1).

A fluid element located at $\mathbf{r}(t)$ has been displaced to the position $\mathbf{r}(t)+\boldsymbol{\xi}(t)$. Lagrangian displacement $\boldsymbol{\xi}$ and Eulerian velocity potential $\delta\phi$ are related by

$$\boldsymbol{\xi} - (\boldsymbol{\xi}.\nabla)\,\mathbf{v} = \nabla\delta\phi. \tag{3.2}$$

For flute instabilities which depend only on the radial and azimuthal space co-ordinates, r and θ, it will be sufficient to consider the radial displacement $\xi(r,\theta,t) = \boldsymbol{\xi}.\mathbf{e}_r$. With the velocity $\mathbf{v} = \dot{r}\mathbf{e}_r$ given by (2.3), equation (3.2) leads to

$$(\xi r)^{\cdot} = r\frac{\partial\phi(r,\theta,t)}{\partial r}. \tag{3.3}$$

With (2.2), one easily finds the Bernouilli equation for the perturbations

$$(\delta\phi)^{\cdot} + \frac{\delta P}{\rho} = 0. \tag{3.4}$$

The isobaric surfaces are of interest for boundary conditions and can be derived from (3.4). Let $\mathbf{r}^* = [r+\xi^*(r,\theta,t)]\,\mathbf{e}_r$ define the perturbed isobaric surface, which experiences the same pressure $\tilde{P}(\mathbf{r}^*,t) = P(\mathbf{r},t)$ as the unperturbed isobaric surface of radius r. At a point $\mathbf{r}$,

$$\delta P = \tilde{P}(\mathbf{r}) - P(\mathbf{r}) = \tilde{P}(\mathbf{r}^* - \xi^*\mathbf{e}_r) - \tilde{P}(\mathbf{r}^*) = -\xi^*\mathbf{e}_r.\nabla P,$$

which gives, with (2.4) and (3.4),

$$\ddot{r}\xi^* = -(\delta\phi)^{\cdot}. \tag{3.5}$$

On the boundaries $r_1(t)$ and $r_2(t)$, which are both fluid and isobaric surfaces, (3.5) holds with $\xi^* = \xi$. Equations (3.3) and (3.5), written for the two boundaries, together with equation (3.1), determine the surface perturbations $\xi_1(\theta,t)$, $\xi_2(\theta,t)$, and the velocity potential $\delta\phi(r,\theta,t)$. The displacements ξ and the isobaric perturbed surfaces should be subsequently obtained with (3.3) and (3.5).

A combination of (3.3) and (3.5) gives on the boundaries

$$(\xi_i r_i \dot{r}_i)^{\cdot} = -r_i\frac{\partial\phi(r_i,\theta,t)}{\partial t} \quad (i=1,2), \tag{3.6}$$

which will be used instead of (3.5). The natural area variable $\eta = \xi r$ appears in both equations (3.3) and (3.6).

3.2. *Harmonic analysis*

The perturbations are Fourier-analyzed in the azimuthal angle θ. The interface radial perturbations $\xi_i = \xi_i(t)\exp ip\theta$ or $\eta_i(t) = \xi_i(t)r_i(t)$ preserve the areas ($i = 1, 2$; $p = 1, 2, 3, \ldots$) and consequently the magnetic pressure P_1. Equations (3.3) and (3.6) are written at the two boundaries, using the order p harmonic solution of (3.1), $\delta\phi = [\alpha(t)r^p + \beta(t)r^{-p}]\exp ip\theta$. They give a linear homogeneous first-order differential system with the variables $\eta_1(t)$, $\eta_2(t)$, $\alpha(t)$ and $\beta(t)$. Eliminating α and β from this system after lengthy algebraic manipulations one gets the following system for the boundary perturbations:

$$\left.\begin{aligned} &\left(\frac{J^{-1}}{p}\dot{\zeta}_1\right)^{\cdot} + b\zeta_1 + c\zeta_2 = 0,\\ &\left(\frac{J}{p}\dot{\zeta}_2\right)^{\cdot} + c\zeta_1 + b\zeta_2 = 0,\\ &\text{where} \qquad \zeta_1 = \eta_2 - \eta_1, \quad \zeta_2 = \eta_2 + \eta_1\\ &\text{and} \qquad J(t) = \frac{\sigma^p - 1}{\sigma^p + 1}, \quad b(t) = \frac{1}{2}\left(\frac{\ddot{r}_2}{r_2} - \frac{\ddot{r}_1}{r_1}\right), \quad c(t) = \frac{1}{2}\left(\frac{\ddot{r}_2}{r_2} + \frac{\ddot{r}_1}{r_1}\right). \end{aligned}\right\} \tag{3.7}$$

The coefficient J is geometrical, depending only on the aspect ratio $\sigma = r_2/r_1$ and on the harmonic number p, while the coefficients b and c (non-independent according to (2.7)) are dynamical and directly related to the accelerations.

Several equivalent systems have been derived, but system (3.7) is the only one which contains interpretable physical quantities while remaining formally relatively simple. However, the following alternative form will also be used:

$$\left.\begin{aligned} &\ddot{u}_1 + I[pbI - (I^{-1})^{\cdot\cdot}]u_1 + pcu_2 = 0, \\ &\ddot{u}_2 + pcu_1 + I^{-1}[pbI^{-1} - \ddot{I}]u_2 = 0, \\ \text{with} \quad &u_1 = I^{-1}\zeta_1, \quad u_2 = I\zeta_2, \quad I = J^{\frac{1}{2}}. \end{aligned}\right\} \tag{3.8}$$

The coefficients of system (3.8) are complicated and are not written explicitly. As the coefficients b and c of system (3.7), they are linear functions of $\ddot{r}_1/r_1$ and $\ddot{r}_2/r_2$.

4. Some stability criteria

Instability is generally understood as an exponential growth of a perturbation. Such is the case when one considers the stability of a fluid or a plasma around an equilibrium or a stationary state. Results are then obtained by a linear normal mode analysis, i.e. taking $\xi \sim \exp(\mathbf{k}.\mathbf{r} + \omega t)$ and examining the sign of $\mathrm{Re}(\omega)$. It is also possible to deduce stability criteria from an energy principle (as did Bernstein *et al.* 1958 and others). The time t is not limited in the linear approximation.

The problem of motion stability is quite different (e.g. Liapounoff 1949; Cotsaftis 1964). Essentially, the motion introduces time-dependent coefficients in the equations of the perturbations, and a normal mode analysis as well as an energy principle formulation is not available any more. Alternatives other than an exponential or sinusoidal behaviour of the perturbations are possible. For example, it should be difficult to consider as stable a perturbation which increases in a monotonic non-exponential way. Moreover, the time t of interest, during which one wants to study the perturbation behaviour, is obviously limited. The definition of stability during a finite time, as well as the definition of the perturbation itself, are relative. For instance, during a converging motion, the perturbation ξ_1 of the inner liner boundary could decrease and then be considered as stable, while the reduced quantity ξ_1/r_1, which characterizes the symmetry departure and which is another measure of the perturbation, could increase and be called unstable.

Owing to all these difficulties it is not surprising that even the linear systems (3.7)–(3.8) cannot be treated in a completely satisfactory way. Let us limit ourselves to enumerating some general properties of these systems, considering an infinite or sufficiently long time; applications will follow in §§ 5 and 6. Analytical solutions exist for only a few cases of interest. When the growth time of the perturbations is small compared with the characteristic time of the motion, a BKW solution will be useful.

4.1. *Properties of a single equation*

Farther on, equations of the form

$$\ddot{y} - nf(t)\,y = 0, \quad f(t) = \left|\frac{\ddot{\bar{r}}}{\bar{r}}\right| > 0 \quad (n = \text{integer}) \tag{4.1}$$

will be found. For $n \gg 1$, or for slowly varying coefficients, they admit the BKW solution

$$y = \frac{1}{f^{\frac{1}{4}}}\left[c_1 \exp\sqrt{(n)}\int^t \sqrt{(f)}\,dt + c_2 \exp -\sqrt{(n)}\int^t \sqrt{(f)}\,dt\right], \tag{4.2}$$

which is asymptotically exponentially unstable when $n > 0$ and stable when $n < 0$ ($f(\infty) \neq 0$). More generally, stability properties depend on the sign of n for a large class of functions f. When $n > 0$ it is always possible to build an unstable monotonic solution of (4.1) which grows without limit. When $n < 0$, the solutions remain bounded and thus stable if f tends monotonically towards a limit $f(\infty) \neq 0$; however, if $f(\infty) = 0$ they can be unstable. As an example, taking $f = \bar{r}_m^2/\bar{r}^4$, which corresponds to the simple A.F.C. hyperbolic motion law (2.13), one gets in terms of $\bar{r}(\bar{t})$ the solution

$$\frac{y}{y(0)} = \bar{r}\left[\cosh(n-1)^{\frac{1}{2}}w + \frac{1}{\bar{r}_m(n-1)^{\frac{1}{2}}}\left(1 + \frac{\dot{y}(0)}{y(0)}\right)\sinh(n-1)^{\frac{1}{2}}w\right], \tag{4.3}$$

where

$$w = \frac{\dot{r}}{|\dot{r}|}\arccos\frac{\bar{r}_m}{\bar{r}} + \arccos\bar{r}_m \quad (\bar{r}_m^2 \ll 1).$$

For $\bar{t} \sim \bar{r} \to \infty$, $f \to 0$ and $y \sim r \to \infty$, whatever n. Nevertheless, the instability is only important for $n > 1$, especially $n \gg 1$, and will be ignored for $n < 1$.

4.2. *Properties of system* (3.7)

It is easy to find the BKW solution of system (3.7), valid for $p \gg 1$ or for slowly varying coefficients:

$$\zeta_1 = F(t)\,\zeta_2 = G(t)\exp(p)^{\frac{1}{2}}\int q(t)\,dt,$$

$$F(t) = -\frac{Jc}{q^2 + bJ} = -\frac{Jq^2 + b}{c}; \quad G(t) = \frac{q}{JF^2}(J^2 + F^2)^{-\frac{1}{2}}. \tag{4.4}$$

The second equation (4.4) gives

$$Jq^4 + (J^2+1)\,bq^2 + J(b^2 - c^2) = 0,$$

which determines $q(t)$. A BKW stability criterion on ζ, based on the sign of $q(t)$, will then be

$$\begin{pmatrix} b < 0 & \text{or} \\ b > 0, & b^2 - c^2 < 0 \end{pmatrix} \rightleftarrows \textit{unstable} \text{ (configurations 1 and 3)},$$

$$(b > 0, \quad b^2 - c^2 > 0) \rightleftarrows \textit{stable} \text{ (configuration 2)}. \tag{4.5}$$

Obviously this criterion is also obtained when the coefficients are supposed to be constant, in which case (4.4) is the exact solution of system (3.7).

When the BKW approximation does not hold, it becomes difficult to get simple results. Nevertheless if $b < 0$ it is possible to find monotone growing solutions for system (3.7). Hence

$$b < 0 \rightarrow \textit{unstable}. \tag{4.6}$$

which is consistent with (4.5). More complete results should involve the derivatives of the coefficients $J(t)$, $b(t)$, $c(t)$. It can also be proved that system (3.8), written in the matrix form $\ddot{\mathbf{u}} + \mathscr{M}\mathbf{u} = 0$, is unstable ($|u|^2$ growing) when $\mathscr{M}$ is a negative definite matrix (see Hartman 1964).

5. Special perturbations study

Before discussing the stability problem it is worth while to consider special cases for which equivalent systems (3.7) or (3.8) split into two independent equations of type (4.1) and are then greatly simplified. Such a simplification occurs for the first-order harmonic $p = 1$ and this trivial case of mere boundary translations will not be analyzed; an obvious equation gives the uniform motion of the centre of gravity. It happens also when the coefficient $J = (\sigma^p - 1)/(\sigma^p + 1)$ is close to its limiting values 0 and 1. This corresponds to wavelengths λ_1 of the inner boundary perturbation, which are small ($J \sim 1$) or large ($J \sim 0$) compared with the liner thickness d. In fact, the wavelength-to-thickness ratio

$$\lambda_1/d = 2\pi/p(\sigma - 1)$$

is equivalent to $\pi(1-J)/J$ for thin liners ($\sigma - 1 \ll 1$), whereas it is necessarily small for thick liners ($\sigma \gg 1$ or $J \sim 1$).

5.1. *Long wavelength perturbations* ($\lambda_1 \gg d$)

The liner has to be thin, which allows one to define the small parameter

$$d/r_1 = \epsilon \ll 1,$$

and to write the long wavelength condition as $p\epsilon \approx 2J \ll 1$. An expansion of system (3.8) in powers of $p\epsilon$ gives at first order ($b \approx O(\epsilon)$, $c = \ddot{r}/r + O(\epsilon)$) the decoupled equations

$$\begin{aligned} (u_1+u_2)^{\cdot\cdot} + (p-1)\frac{\ddot{r}}{r}(u_1+u_2) &= 0, \\ (u_1-u_2)^{\cdot\cdot} - (p+1)\frac{\ddot{r}}{r}(u_1-u_2) &= 0, \end{aligned} \tag{5.1}$$

where

$$u_1 \approx \frac{2r^2}{sp^{\frac{1}{2}}}(\xi_2 - \xi_1), \quad u_2 \approx sp^{\frac{1}{2}}\frac{\xi_1+\xi_2}{2} \quad \text{and} \quad r = r_1 \approx r_2.$$

According to the conclusions of § 4.1, at least one of these equations will have an *unstable* solution, whatever the sign of r. As can be seen by considering the two modes $u_2 = \pm u_1 = c^t \times \xi$, the mean displacement $\xi = \frac{1}{2}(\xi_1 + \xi_2)$ is always unstable, while the thickness variation $\Delta d = \xi_2 - \xi_1$ is asymptotically related to ξ by $\Delta d/d \approx \pm 2\pi\xi/\lambda$. Agreement with the BKW criterion, which should result

in stability for a configuration 2, is thus not complete. However, for a configuration 2 and a thin liner the accelerations are so small that the BKW analysis, as well as the present approximation, are no longer valid. Configuration 2 is slowly or marginally unstable ($\ddot{r} \sim 0$).

When the thickness d tends to zero the Rayleigh–Taylor instability is better analyzed in terms of radial and azimuthal displacements $\xi_r(t)\exp(ip\theta)$ and $\xi_\theta(t)\exp(ip\theta)$. Equations for displacements are directly derived and turn out to be equations (5.1), taking $\xi_r = u_2/sp^{\frac{1}{2}}$ and $\xi_\theta = iu_1/sp^{\frac{1}{2}}$.† Hence, $|\xi_\theta|$ is the limit of the quantity $r|\xi_2-\xi_1|/pd$, when $d \to 0$. The stability problem is completely solved for A.F.C. by infinitely thin liners. The motion law is (2.13) and equations (5.1) have solutions of type (4.3).

Such solutions still give an approximation for A.F.C. by thin liners. They are straightforward but rather cumbersome and will not be written. Using reduced initial perturbations $\bar{\xi}_i(0) = \xi_i(0)/r_1(0)$ and $\dot{\bar{\xi}}_i(0) = \dot{\xi}_i(0)/\dot{r}_i(0)$ one finds that the geometrical ratio ξ/r is amplified up to the value

$$\left(\frac{\xi}{r}\right)_m \sim \frac{1}{4D\bar{r}_m}\{(1-\bar{r}_m p^{\frac{1}{2}})[\bar{\xi}_2(0)-\bar{\xi}_1(0)]+\dot{\bar{\xi}}_1(0)-\dot{\bar{\xi}}_2(0)\}\frac{\exp(\frac{1}{2}\pi p^{\frac{1}{2}})}{p^{\frac{3}{2}}} \tag{5.2}$$

at the maximum compression and tends towards a maximum

$$(\xi/r)_{\max} \sim (\xi/r)_m \exp(\tfrac{1}{2}\pi p^{\frac{1}{2}})$$

when $\bar{r} \sim \bar{t} \to \infty$ (first-order approximation in ϵ and D).

5.2. *Short wavelength perturbations*

From the short wavelength condition one gets the expansion parameter

$$1-J \approx 2\sigma^{-p} \ll 1.$$

The liner may be thick as well as thin, but for thin liners one has necessarily $p \gg 1$. A development of system (3.8) gives at zero order in σ^{-p} the decoupled equations

$$\ddot{\eta}_2 + p\frac{\ddot{r}_2}{r_2}\eta_2 = 0; \quad \ddot{\eta}_1 - p\frac{\ddot{r}_1}{r_1}\eta_1 = 0. \tag{5.3}$$

The perturbation $\eta_i = r_i\xi_i$ is then unstable (§ 4.1) on a boundary towards which the acceleration is directed ($\ddot{r}_1 > 0$ or $\ddot{r}_2 < 0$, configuration 1 or 3), and the first-order approximation shows also that the perturbation η_j on the other boundary is of the order of $\sigma^{-p}\eta_i$. Such an instability cannot develop on both boundaries: the case $\ddot{r}_1 > 0, \ddot{r}_2 < 0$ has been excluded in § 2.1. For a configuration 2 (e.g. free liners or equal pressures on the boundaries), $\ddot{r}_1 < 0, \ddot{r}_2 > 0$ and the perturbations η_i oscillate; according to the results of § 4.1 they are stable.

It will be noticed that equations (5.3) have the same form as equations (5.1) for long wavelengths, but the variables are the $\eta_i = r_i\xi_i$ instead of the displacements ξ_i. Short and large wavelength perturbations have thus very different

† Harris (1962) studied the Rayleigh–Taylor instability of infinitely thin cylindrical shells but forgot the term $\mathbf{e}_\phi\,\xi_\phi\,d\phi\,dz$ in his equation (3.8) and consequently derived different equations.

behaviours. As shown by the solutions of (5.1) and (5.3) taken for $\ddot{r}_1 = 0$, a geometrical effect tends to amplify the short wavelength perturbations more than the long ones in a converging motion, while the opposite is true for a diverging motion. However, in the presence of accelerations the two kinds of perturbations have different growth times (roughly proportional to $p^{-\frac{1}{2}}$) and this effect is not generally apparent.

In the A.F.C. case the rough motion law (5.13) gives again an analytical solution of type (4.6). The perturbation amplitude $|\xi_1|$ has the approximate value, at maximum compression,

$$|\xi_1|_m \approx \tfrac{1}{2}\left|\xi_1(0)+\frac{\dot{\xi}_1(0)}{\bar{r}_m p^{\frac{1}{2}}}\right| \exp\left(\frac{\pi}{2}p^{\frac{1}{2}}\right) \quad (p \gg 1) \tag{5.4}$$

and tends asymptotically towards a limit $|\xi_1|_{\max} \approx |\xi_1|_m \exp(\frac{1}{2}\pi p^{\frac{1}{2}})$ in the diverging motion phase. It is not strictly unstable (only η is unstable) but reaches extremely large values. The geometrical ratio $|\xi_1/r_1|$ has a sharp maximum near the turn-around radius and tends asymptotically towards zero.

5.3. *Discussion*

The general results obtained in § 4.2 for the asymptotic stability of system (3.7) are summarized in figure 2, where the three possible configurations, distinguished in § 2 for the unperturbed motion, have been reported. For $b > 0$ only a BKW criterion exists but the study of special perturbations has just shown that BKW unstable configurations 1 or 3 remain unstable even in cases for which BKW criterion does not necessarily apply. Some doubt remains about the only region of possible stability, configuration 2, which could be slightly unstable for long wavelengths. However, configuration 2 is relative to small pressure differences $(P_1 - P_2) < \frac{1}{2}\rho v_1^2$, and to small accelerations, and is not important in practice.

The instability of the perturbations is consequently a general rule for radial cylindrical motions. In A.F.C. the motion is initially a configuration 2 or 1 with small accelerations and then starts to be oscillating or slightly unstable. At maximum compression the coefficient b has a large negative value (table 1) and the motion belongs to the always unstable configuration 1. For our purpose it is essential to evaluate the development of given initial perturbations. The results of this section will suffice for only extreme cases. For most experimental cases the simplified motion law (2.13) is inappropriate and the perturbations generally do not remain in a region of long or short wavelengths during the whole compression. Thus formulas (5.2) and (5.4) have a limited validity range and a numerical resolution of system (3.7) is necessary.

6. Instability of axial field compressions

System (3.7) has been solved numerically using the A.F.C. motion law (2.11) and considering four independent sets of initial reduced perturbations determined by the quantities $(\bar{\xi}_1(0), \dot{\bar{\xi}}_1(0), \bar{\xi}_2(0), \dot{\bar{\xi}}_2(0))$. The harmonic p varies between 1 and 100. A basic case A has been chosen ($\bar{r}_m = 0{\cdot}1, D = 4 \times 10^{-2}$ or $N = 4 \times 10^{-4}$;

table 1), which corresponds to various experimental devices (for example to

$$r_1(0) = 5\,\text{cm}, \quad r_2(0) = 5{\cdot}2\text{cm}, \quad \dot{r}_1(0) = -2\times 10^5\,\text{cm/s},$$

$$B(0) = 6\times 10^4 G, \quad B_m = 6\times 10^6 G;$$

copper liner). Special attention has been paid to the significant geometrical quantity $g(\bar{t}) = \bar{\xi}_1/\bar{r}_1$, which is a measure of the asymmetry.

The behaviour of the spatial inner boundary mode (1, 0, 0, 0) is considered first. Results relative to a small and a large p are given by figure 4.† For $p = 2$ the agreement with the theory developed in § 5.1 on long wavelength perturbations is qualitatively good, and (5.2) gives a reasonable estimate of $|g|_m$; nevertheless the perturbation wavelength λ_1 becomes smaller than the thickness at maximum compression, and the theoretical value for $|g|_{\max}$ is very rough. For $p = 100$ the outer boundary perturbation remains negligible and $|g|$ has a maximum, as would be expected from the small wavelength perturbation theory of section (5.2). However, the value (5.4) of $|g|_m$ is overestimated by three orders of magnitude, and it may be concluded either that the initial wavelength is not small enough or that, for fast-growing perturbations, the motion law (2.13) is too rough to justify the first-order theory.

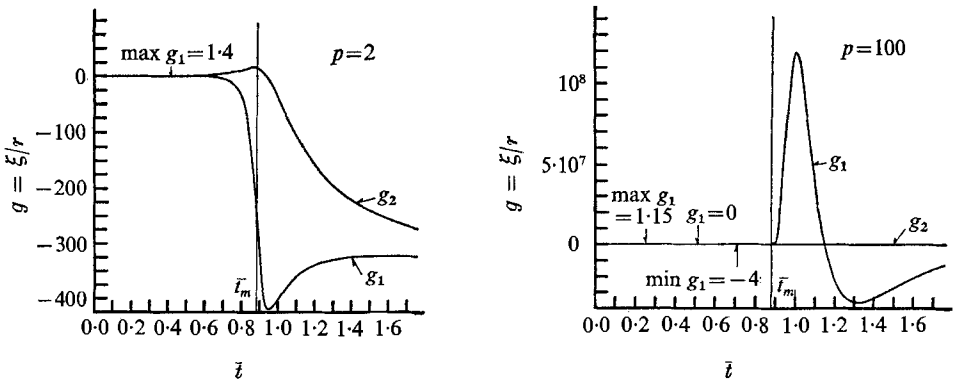

FIGURE 4. Boundary instability for A.F.C., case A ($\bar{r}_m = 0{\cdot}1$, $D = 4\times 10^{-2}$), initial pertubation mode (1, 0, 0, 0) and harmonics $p = 2$ and 100.

Results are clearer in figure 5, which gives the dependence of the geometrical ratio $|g|$ on the harmonic number p. Three values of $|g(\bar{r}_1, p)|$ are plotted for every p and are relative to the radius $r_1 = 1{\cdot}43 r_m$ (in the compression phase), to the turn-around radius r_m and to the maximum value $|g|_{\max}$. Such a maximum value always exists, reached in the decompression phase for a variable radius $r_1 \lesssim 2r_m$ and will thus measure the over-all instability effects. Figure 5 implies the following:

(i) Whatever p, the instability does not develop during the main part of the motion (curve for $r_1 = 1{\cdot}43 r_m$). Accelerations then being small, oscillating and slowly unstable modes are mixed. A resonance between a minimum of the

† More results can be found in Somon (1968*a*).

perturbation and the beginning of the acceleration peak explains the holes which appear on the curves ($g(p)$ changes sign at the resonance).

(ii) At the maximum compression the instability starts to be important and increases with the harmonic number. Owing to the acceleration peak it becomes extremely high just after the maximum compression.

(iii) Figure 5 illustrates the behaviour of the other modes. Low-order harmonics ($p \lesssim 10$) develop in a closely similar way for all modes and curves can be almost superimposed. High-order harmonics relative to the outer boundary modes (0, 0, 1, 0) or (0, 0, 0, 1) grow much less than those relative to the inner boundary modes (1, 0, 0 ,0) or (0, 1, 0, 0).

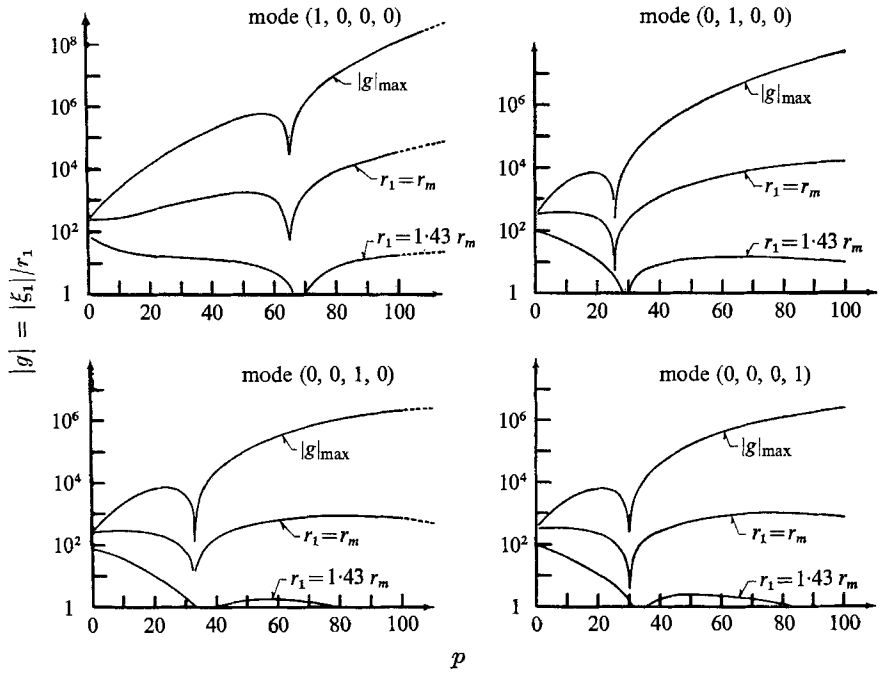

FIGURE 5. The geometrical ratio $|g| = |\xi_1|/r_1$ of the inner boundary displacement over radius as a function of the harmonic number p. The curves are relative to radius $r_1 = 1{\cdot}43 r_m$ (converging phase), turn-around radius $r_1 = r_m$ and to the maximum value $|g|_{max}$ of $|g|$, reached at the beginning of the decompression phase. Four independent initial perturbation modes ($\xi_1(0)$, $\dot{\xi}_1(0)$, $\xi_2(0)$, $\dot{\xi}_2(0)$) are considered. The non-perturbed motion is case A of axial field compression ($\bar{r}_m = 0{\cdot}1$, $D = 4 \times 10^{-2}$).

Other cases B, C, D, E have been calculated in order to estimate the effect the reduced thickness D and turn-around radius $\bar{r}_m$ have on the instability. Figure 6 and table 1 give some results. Comparison of the cases B, A, C with the same turn-around radius $\bar{r}_m = 0{\cdot}1$ shows that, when the thickness is smaller, the instability is greater. This effect is more noticeable for high-order harmonics and initial perturbations located on the outer boundary. The influence of the compression magnitude is seen from the cases D, A, E relative to the same thickness $D = 0{\cdot}04$. When the turn-around radius decreases, low-order harmonics become more unstable (according to (5.2)) and, conversely, high-order harmonics less unstable.

	A	B	C	D	E
D	0·04	0·1	0·01	0·04	0·04
$\bar{r}_m$	0·1	0·1	0·1	0·25	0·05

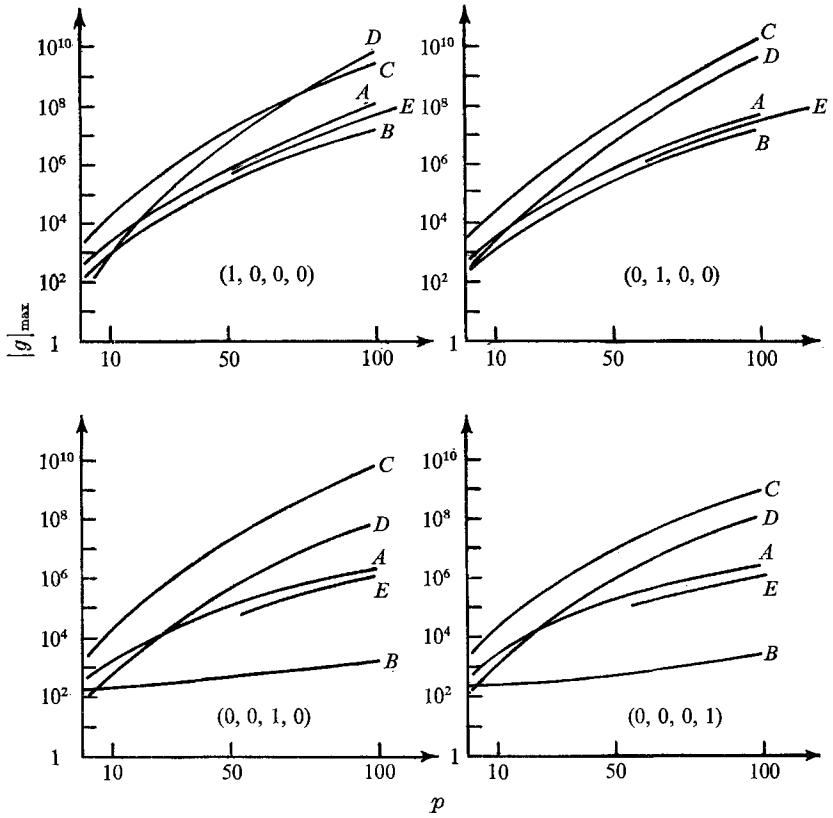

FIGURE 6. The maximum $|g|_{max}$ of the geometrical ratio $|\xi_1/r_1|$ of the inner boundary displacement over radius as a function of the harmonic number p. Four initial perturbation modes ($\bar{\xi}_1(0)$, $\dot{\bar{\xi}}_1(0)$, $\bar{\xi}_2(0)$ $\dot{\bar{\xi}}_2(0)$) and five A.F.C. non-perturbed motions are considered. Curves are based on a few points and have only an indicative character.

Conclusion: conditions for liner destruction

The calculations presented allow one, through Fourier analysis and mode decomposition, to evaluate at any time the liner symmetry departure $|\xi_1|/r_1$ relative to every given initial perturbation. Conversely, it is possible to determine the initial perturbations which become dangerous during the compression. Instability will be tolerable as long as $|\xi_1|/r_1$ remains smaller than unity, i.e. the compression is not destroyed by a perturbation reaching the axis. For each of the preceding modes, this condition for non-destruction at time t can be written as

$$\left|\frac{\xi_i(0)}{r_1(0)}\right| < \frac{1}{|g(t)|} \quad \text{or} \quad \left|\frac{\dot{\xi}_i(0)}{\dot{r}_1(0)}\right| < \frac{1}{|g(t)|}. \tag{6.1}$$

Note that the perturbation-to-wavelength ratio becomes $|\xi_1|/\lambda_1 = \frac{1}{2}p/\pi$ when the liner is destroyed or $|\xi_1|/r_1 = 1$. Linear approximation is expected to be still

roughly valid if this ratio is smaller than unity. Condition (6.1) will then hold only for low-order harmonics ($p \lesssim 10$), which correspond to the most important liner gross deformation. For high-order harmonics non-linear effects lead to the formation of jets or droplets long before the destruction limit is reached. The large p linear perturbations have thus no great physical meaning, and the magnetic field diffusion, which could vaporize jets and drops, adds to their complexity. Let us now discuss the case A, taking $r_1(0) = 5\,\text{cm}$, $d(0) = 2\,\text{mm}$ and initially given inner boundary ripples or type (1, 0, 0, 0) perturbations.

As demonstrated, the motion does not exhibit large instabilities in the converging phase, for radii r_1 somewhat greater than the turn-around radius r_m. Even for the radius $r_1 = 1{\cdot}43 r_m$, at which the magnetic field reaches about half its maximum value, $|g(p)|$ has a mean value of 20 and the symmetry is still very good if $|\xi_1(0)| \gg 2{\cdot}5\,\text{mm}$, a condition which is obviously achieved in normal implosions. This is in agreement with experimental results.

Close to the maximum compression, instability starts to grow rapidly and, at the turn-around radius, condition (6.1) for non-destruction becomes

$$|\xi_1(0)| \lesssim 0{\cdot}2, 0{\cdot}15, 1{\cdot}4 \times 10^{-3}\,\text{mm}$$

for the respective harmonics $p = 2, 10, 100$. The initial perturbations are not well known and they should be related in some way to the symmetry characteristics of each experimental liner-explosive device. Nevertheless, even discarding harmonic 100, the smallness of the figures relative to harmonics 2 and 10 is such that the condition for non-destruction will be difficult to satisfy. The existence of the turn-around radius or maximum compression is then doubtful but possible. Available experimental data confirm such a conclusion.

At the very beginning of the decompression phase the asymmetry reaches its maximum $|g|_{\max}$, which gives the condition of non-destruction during the whole motion $|\xi_1(0)| \lesssim 0{\cdot}16,\ 0{\cdot}02,\ 5 \times 10^{-7}\,\text{mm}$, again for $p = 2, 10, 100$. This condition is much more stringent than the turn-around one as soon as the harmonic order increases. The liner will consequently be quite certainly destroyed by motion instability just after the maximum compression should it occur. Indeed, the decompression phase has never really been observed in experiments.

These conclusions do not depend much on the considered mode. On the other hand, the liner characteristics do not enter strongly, as shown by table 1, where cases C and D must be considered extreme and somewhat unrealistic. However, due to the critical increase of $|g(t)|$ near maximum compression, each experimental case must be examined carefully.

7. Large-amplitude instability of a compressible liner (A.F.C.)

Let us now come back briefly to the two fundamental hypotheses of small-amplitude perturbations (linearization) and liner incompressibility which are the basis of the preceding A.F.C. instability calculations. As the amplitude of a harmonic perturbation grows, non-linear effects couple gradually higher harmonics and the perturbation-shape changes. Narrowing spikes and broadening bubbles appear and develop respectively faster and slower than the perturbation

predicted by the linear theory. Following Harlow & Welch (1966), non-linear effects appear when $|\xi|/\lambda$ becomes greater than 0·4, in the plane case. Conclusions of § 6, where the linearity limit $|\xi_1|/\lambda_1 \lesssim 1$ was chosen arbitrarily, could then be altered for large-amplitude perturbations. On the other hand, metallic liners are slightly compressible ($\rho_0 \leqslant \rho \leqslant 2{\cdot}5\rho_0$) at megabar magnetic pressures. Somon (1965) proved that the incompressibility assumption (motion law 2.11) is valid when the reduced liner thickness D is somewhat smaller than a critical thickness $D_c = N^{\frac{1}{2}}(1{\cdot}5 + 1/M)^{\frac{1}{2}}$ ($M = |\dot{r}_1(0)|/c(0)$, $c(0)$ = initial sound velocity). For most compressions the unperturbed motion is only slightly influenced by the compressibility ($D \sim D_c, B_m \sim$ some megagauss). However, for large compressions ($D > D_c$, higher B_m) a shock wave is created within the liner and the compressibility influence is not negligible any more; maximum field and accelerations are smaller, but last longer than they would if the liner were incompressible.

In order to take these effects into account, a numerical technique has been used to solve the full non-linear, fluid equations (dependent on time and two space co-ordinates) for a compressible non-viscous fluid. The numerical method, called M.I.G. ('Méthode des Intégrales Généralisées'), works well for low-harmonic perturbations, but consumes a prohibitive computer time as soon as $p > 10$ (Guerri & Stella). The equation of state for the liner is the same as that in a previous paper (Somon 1965). Magnetic flux conservation still gives the inner boundary condition. The following results are relative to the initial harmonic perturbation of the inner boundary

$$\tilde{r}_1(0) = r_1(0) + \mu[r_2(0) - r_1(0)]\cos p\theta, \quad \tilde{r}_2(0) = r_2(0), \tag{7.1}$$

with

$$\tilde{v}(r, 0) = v(r, 0) = v_2(0)\, r_2(0)/r, \quad P(r, 0) = 0.$$

They will be compared with the predictions of the preceding linear incompressible theory, corresponding to the reduced mode $(\mu D, \mu D, 0, 0)$.

Numerical results

It would be desirable to study a quasi-incompressible case, with $D \ll D_c$, in order to dissociate variations due to non-linearity and compressibility. A more realistic case, corresponding to an experimental device, has been preferred. Determined by

$$r_1(0) = 4{\cdot}8\,\text{cm}, \quad r_2(0) = 5\,\text{cm}, \quad v_2(0) = 2 \times 10^5\,\text{cm/s}, \quad B(0) = 6{\cdot}5 \times 10^4\,\text{G} \tag{7.2}$$

and a copper liner, it does not appreciably differ from the basic case A of § 6. The initial thickness is $D = 1{\cdot}08 D_c$ and the compressibility influence is thus small but not completely negligible. In fact the unperturbed maximum compression values $B_m = 5{\cdot}06$ MG, $r_m = 0{\cdot}54$ cm are slightly different from the incompressible values $B_m = 6{\cdot}15$ MG, $r_m = 0{\cdot}49$ cm given by (2.12). Instability behaviour is shown in figures 7–10 and can be followed for increasing initial perturbation or μ.

(i) For small μ ($\mu = 0{\cdot}02$, $p = 2$; figure 7) the perturbation follows the linear incompressible theory predictions until the end of the compression phase. Spikes and bubbles appear afterwards. A spike grows less than linearly (smaller accelerations due to compressibility) before exceeding the linear behaviour (higher

harmonics coupling). The bubble amplitude always remains smaller than the spike and linear amplitudes. Successively, bubbles are repelled ($r_1 = 0{\cdot}58$ cm; $t = 20{\cdot}38\,\mu$s), the field reaches a maximum (5·07 MG, $t = 20{\cdot}58\,\mu$s), and spikes are repelled ($r_1 = 0{\cdot}50$ cm, $t = 20{\cdot}78\,\mu$s). In this slightly perturbed compression the magnetic field $B(t)$ never differs more than 0·2 % from the unperturbed field.

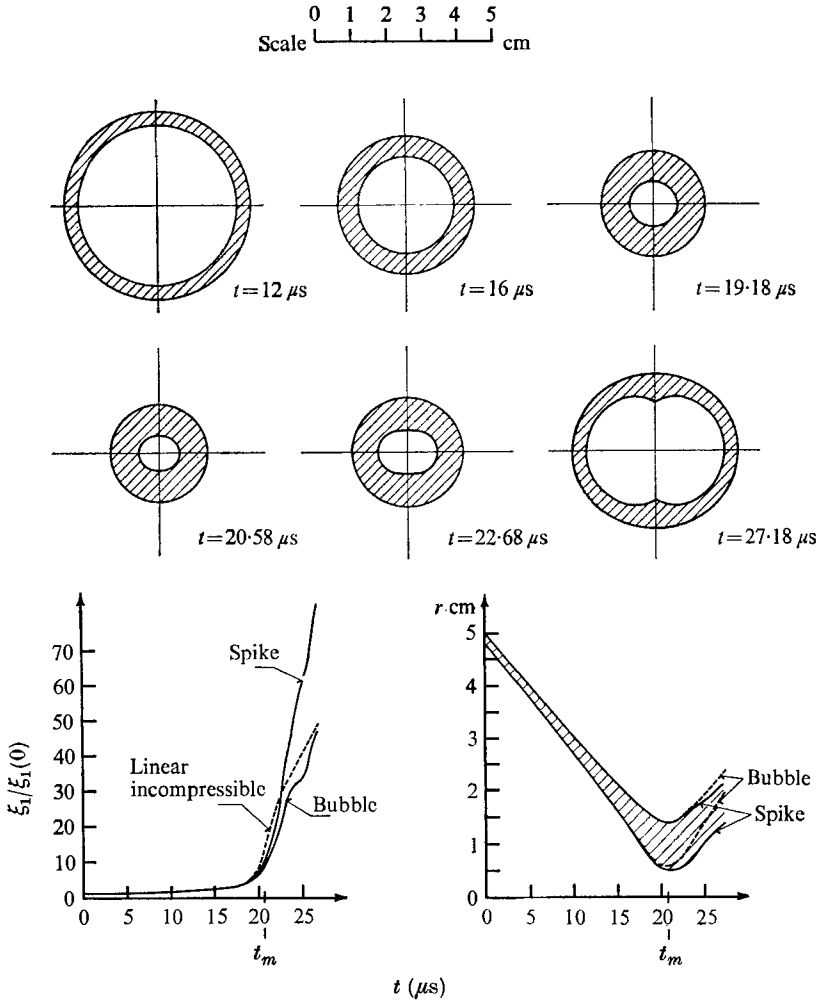

FIGURE 7. Behaviour of Rayleigh–Taylor instability given by the numerical resolution of the full fluid equations for axial field compression (7.2) and initial perturbation (7.1), harmonic $p = 2$ with $\mu = 2 \times 10^{-2}$. The dashed curve for the inner boundary perturbation is relative to the corresponding linear incompressible reduced mode (μD, μD, 0, 0).

(ii) When the initial perturbation increases, spikes come closer to the axis, which they reach for a value $\mu = \mu^*$. The liner is then destroyed after the maximum compression. One finds $\mu^* \approx 0{\cdot}06$ for $p = 2$ and $\mu^* \approx 0{\cdot}03$ for $p = 6$. Using $|g|_{\max}$, comparable conditions for the destruction of the linear incompressible theory should give the higher values $\mu^* = 0{\cdot}16$ and 0·05. Obviously

the spikes have a greater amplitude than the linear perturbation when they reach the axis. Figures 8 and 9 illustrate the development of destructive instabilities.

(iii) A further increase of the initial perturbation leads to a value $\mu = \mu^{**}$ above which spikes reach the axis and destroy the liner before a maximum field has been reached. Nevertheless bubbles have already been repelled by the field pressure. For $p = 2$ and 6 one obtains $\mu^{**} \approx 0{\cdot}2$ and $0{\cdot}15$, which do not greatly differ from the linear incompressible theory values $0{\cdot}22$ and $0{\cdot}17$ calculated with $|g|_m$. Indeed, spikes had no time to develop much more than linear perturbations for these early liner destructions.

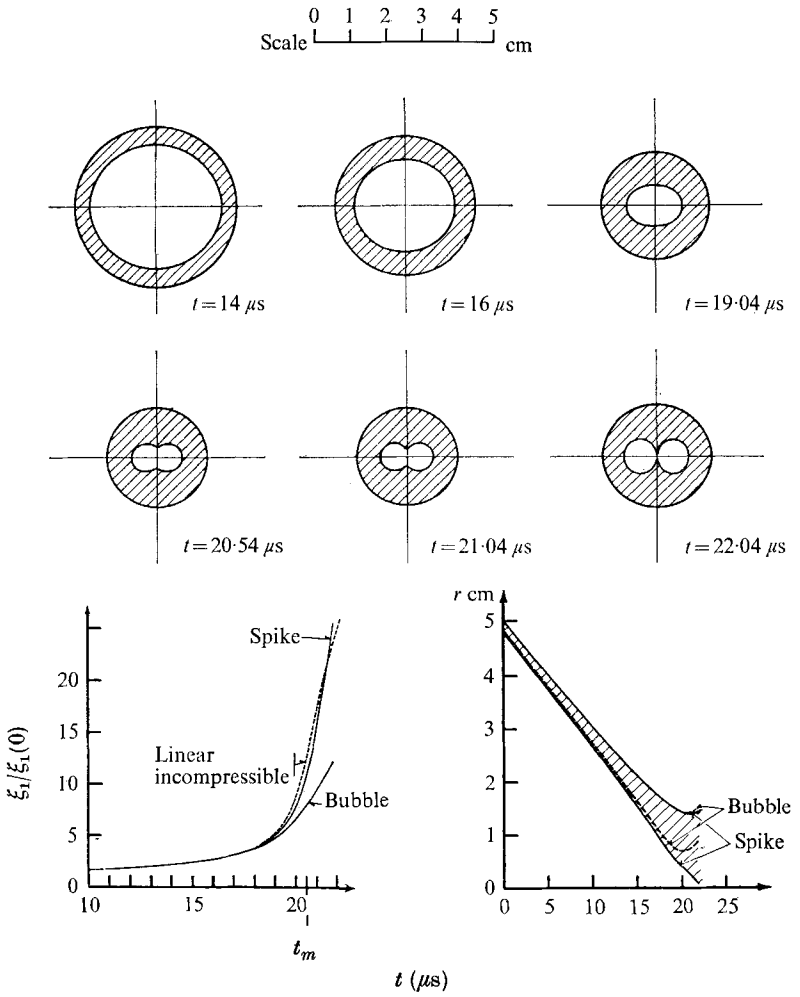

FIGURE 8. Analogue of figure 7, with $p = 2$ and $\mu = 0{\cdot}1$.

(iv) The perturbed magnetic field behaviour shown in figure 10 is particularly interesting. The instability effect is found to diminish the maximum field amplitude and to narrow or even eliminate the magnetic peak. It could explain the dispersion of magnetic signals obtained by probe measurements.

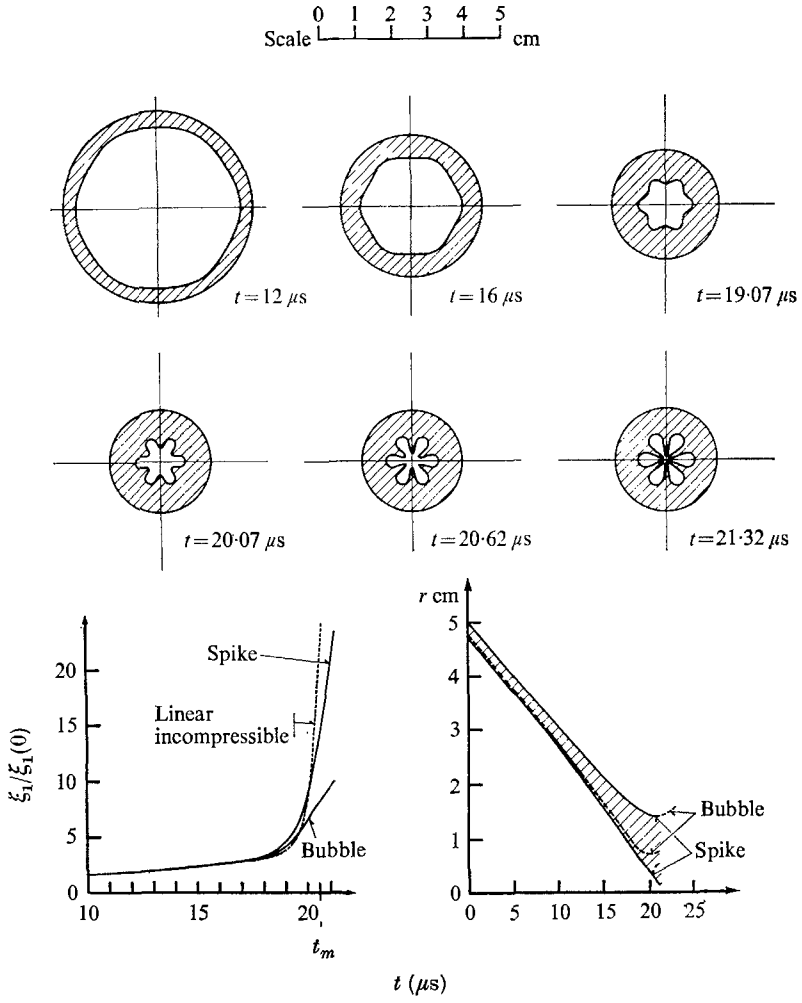

FIGURE 9. Analogue of figure 7, with $p = 6$ and $\mu = 0{\cdot}1$.

It may be concluded that the linear-incompressible theory predicts well the initial perturbations for which the instability destroys the liner before the maximum field has been reached (values relative to $|g|_m$ or μ^{**}). Less accurate are the conditions for destruction in the decompression phase. Values of $|g|_{\max}$ are underestimated in the linear theory but they could be used with a safety coefficient of about 3. Such a conclusion should be generally valid for $D \lesssim D_c$ and low-order harmonics.

Great confidence in the linear incompressible theory cannot be expected when compressibility plays a more important role. For example, let us modify initial condition (7.2) by taking $v_1(0) = 8 \times 10^5$ cm/s, $B(0) = 1{\cdot}5 \times 10^5$ G, which gives $D/D_c = 2{\cdot}34$. One obtains a maximum field $B_m = 20{\cdot}9$ MG and a turn-around radius $r_m = 0{\cdot}41$ cm, which greatly differ from the incompressible values $B_m = 40$ MG and $r_m = 0{\cdot}29$ cm. Perturbations of type (7.1) have again been

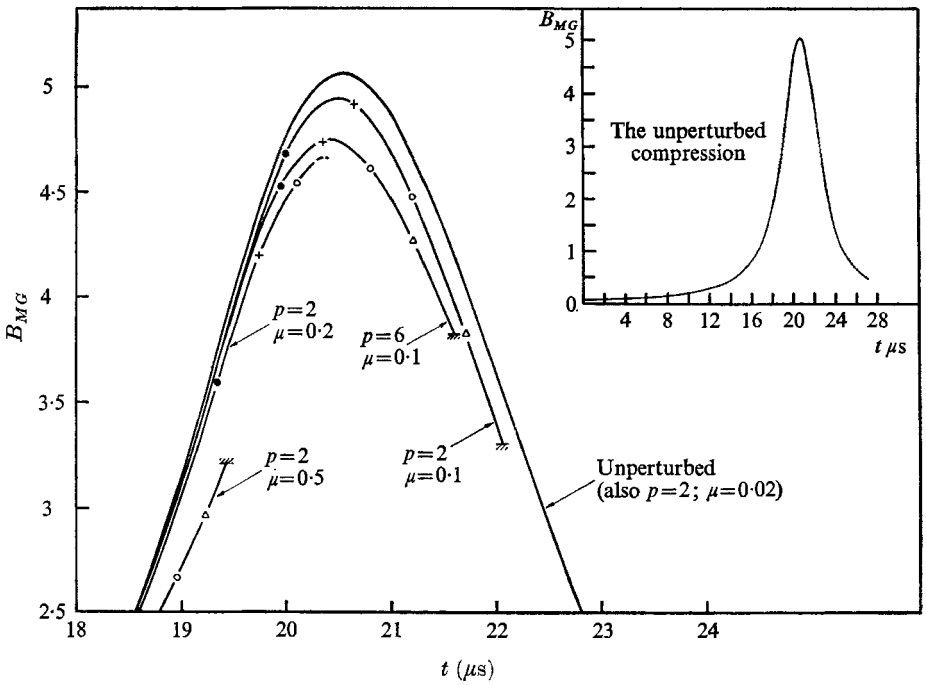

FIGURE 10. Effect of instability on magnetic field amplification as given by the numerical resolution of the full fluid equations for A.F.C. (7.2) and several initial perturbations of type (7.1). The points indicated on the magnetic field versus time curves allow one to follow the development of the spikes. Points indicating the spike distance to the axis (r_m = 0·543 cm): ●, 0·4 cm; +, 0·3 cm; ○, 0·2 cm; △, 0·1 cm; ▨, 0·0 cm.

considered for $p = 2$ and $p = 6$. Numerical results show that the linear incompressible theory remains valid until the maximum compression vicinity, i.e. obviously as long as the magnetic pressure is not too high, but may lead afterwards to erroneous perturbation behaviour. For instance, when $p = 6$, the linear incompressible perturbation changes sign close to the maximum compression; as explained in § 6, this is due to the occurrence of oscillating modes, and resonance holes should appear for $p < 6$ on the $|g(p)|$ curves, analogous to those of figure 5. Such a phenomenon is not observed if the compressibility is taken into account. The perturbation always grows, and holes seem not to occur. Calculation gives the critical $\mu^* \approx 0{\cdot}04$ and 0·015, $\mu^{**} \approx 0{\cdot}15$ and 0·15, for $p = 2$ and 6 respectively. Critical μ are then comparable to those of the very different case (7.2). As has already been noticed for the linear incompressible theory, the conditions for liner destruction do not seem to depend very much on the considered case.

The author is grateful to Dr J. G. Linhart for having encouraged this work, and thanks Dr G. Di Cola for fruitful discussions and for the numerical treatment involved in § 6. The M.I.G. method mentioned in § 7 was developed by the S.E.M.A. Society in Paris. The author also thanks Drs L. Guerri and P. Stella-Fasoli, who improved this method and obtained the numerical results of § 7.

REFERENCES

AL'TSCHULER, L. V. 1965 *Uspekhi* **8**, 52.

BERNSTEIN, I. B., FRIEMAN, E. A., KRUSKAL, M. D. & KULSRUD, R. M. 1958 *Proc. Roy. Soc.* A **244**, 17.

BIRKHOFF, G. 1956 *Los Alamos Scientific Laboratory Report* LA 1927.

CESARI, L. 1963 *Asymptotic Behaviour and Stability Problems in Ordinary Differential Equations*. Berlin: Springer.

CHAMPETIER, J.-L., LARGER, J.-C., LECHANCHE, Y. & NELSON, P. 1965 *C. R. Acad. Sci., Paris.* **261**, 2825.

CHANDRASEKHAR, S. 1961 *Hydrodynamic and Hydromagnetic Stability*. Oxford: Clarendon Press.

COTSAFTIS, M. 1968 *J. Inst. Maths. Applics.* **5**, 19.

DI GREGORIO, C., HERLACH, F. & KNOEPFEL, H. 1966 *Proc. Conf. on Megagauss Magnetic Field Generation by Explosives and Related Experiments*, Frascati 1965. Brussels: EURATOM 2750e.

EMMONS, H. W., CHANG, C. T. & WATSON, B. C. 1960 *J. Fluid Mech.* **7**, 177.

GUERRI, L. & STELLA, P. *EURATOM Ispra.* (To be published.)

HARLOW, F. H. & WELCH, J. E. 1966 *Phys. Fluids* **9**, 842.

HARRIS, E. G. 1962 *Phys. Fluids* **5**, 1057.

HARTMAN, P. 1964 *Ordinary Differential Equations*. New York: Wiley.

JAREM, J. & WATSON, M. 1962 *Proc. Vth Int. Conf. on Ionization Phenomena in Gases, Munich*. Amsterdam: North Holland.

KRUSKAL, M. & SCHWARZSCHILD, M. 1954 *Proc. Roy. Soc.* A **223**, 348.

LEHNER, G., LINHART, J. G. & SOMON, J. P. 1964 *Nuclear Fusion* **4**, 362.

LIAPOUNOFF, M. A. 1949 *Probléme général de la stabilité du mouvement.* Princeton University Press.

LINHART, J. G. 1961 *J. Appl. Phys.* **32**, 500.

PLESSET, M. S. 1954 *J. Appl. Phys.* **25**, 96.

RAYLEIGH, J. W. S. 1900 *Scientific Papers*, vol. II. Cambridge University Press.

SOMON, J. P. 1966 *Proc. Conf. on Megagauss Magnetic Field Generation by Explosives and Related Experiments, Frascati* 1965. Brussells: EURATOM 2750e.

SOMON, J. P. 1968*a* *Laboratori Gas Ionizzati Report* LGI 68/4.

SOMON, J. P. 1968*b* Sur l'obtention de champs magnétiques intenses au moyen d'une implosion cylindrique. Thèse de Doctorat és Sciences, *Euratom Report EUR* 4197f.

TAYLOR, G. 1950 *Proc. Roy. Soc.* A **201**, 192.

WEHAUSEN, J. V. & LAITONE, E. V. 1960 *Encyclopedia of Physics*, vol. III. *Fluid Dynamics*. Berlin: Springer.